

We feel very grateful to the reviewer who has given us the valuable suggestions and comments for our paper. We have revised our manuscript accordingly.

Huayong Chen

Responses to the reviewer' comments:

Comments of Anonymous Referee #1:	Author's Reply
<p><b>1.</b> p.1, line 2 not sure, if "downriver of a check dam" would better describe the exact location of the scour.</p>	<p>Thanks very much for the reviewer's comment. The phrase "behind a check dam" has been replaced by "downriver of a check dam" for better description of the exact scour location.</p>
<p><b>2.</b> p.1, line 11 in cases where debris flow is used in a word composition (e.g. debris-flow pattern, debris-flow nappe) I learned, that there is a hyphen between debris and flow Please check the manuscript accordingly.</p>	<p>A hyphen was added between debris and flow in a sentence throughout the manuscript where "debris flow" was used as attributive.</p>
<p><b>3.</b> p.2, line 29 more common is "initiation zone", not "formation region"; delete "by debris flow" at the end of the sentence, it's an unnecessary repetition.</p>	<p>The wrong phrases in the sentence have been revised according to the reviewer's comments.</p>
<p><b>4.</b> p.3, line 56/57 not really clear, what this sentence means. Do you mean that the proposed geometry of such spillways is something that should be used especially for torrents with high sediment disposability?</p>	<p>To avoid misunderstanding, the sentence has been modified in the manuscript.</p>
<p><b>5.</b> p.3, line 58 "is" instead of "was".</p>	<p>The word "was" has been replaced by "is" in this sentence.</p>
<p><b>6.</b> p.8, line 165 are the values for the density of the debris-flow densities measured values or assumptions? Both values seems to me more valid for hyperconcentrated flows. I would</p>	<p>The flow densities were measured after debris-flow samples were taken. Frankly, as for debris flows the flow density in our experiments seems lower. The experimental analy-</p>

<p>espect values in the order of 1700 - 1900 kg/m<sup>3</sup>.</p>	<p>sis here is considered to be the preliminary achievements. The authors appreciate the reviewer's valuable suggestions to carry out more experiments involving debris-flow densities in the order of 1700 - 1900 kg/m<sup>3</sup> in the future.</p>
<p><b>7.</b> #1: indicate flow direction and exchange the word "behind" with "downriver of".</p>	<p>The word "behind" has been replaced by "downriver of".</p>
<p><b>8.</b> #2a: Sabo dam is never use in the text. Use check dam or replace check dam with sabo dam in the text.</p>	<p>The word "Sabo dam" has been replaced by "check dam".</p>
<p><b>9.</b> #5: describe it as "debris-flow hydrograph". If your LRF gave you min, max and mean values, you could perhaps explain the outliers. And: this hydrograph does not really show a typical steep front of a debris flow. It looks more like a hyperconcentrated flood. Again: add information on the sampling rate of the device.</p>	<p>The caption of Figure 5 was changed to "debris-flow hydrograph". The information on the sampling rate of the device was added in line 90, page 5.</p>
<p><b>10.</b> #6: add an arrow to show flow directions. Very small images. Perhaps increase contrast.</p>	<p>An arrow in each figure was added to show debris-flow directions in Fig.6.</p>
<p><b>11.</b> Scaling effects are not discussed. Please add a section to explain how the results of the experiments can be use in real dimensions. What is the Froude number of your experiments?</p>	<p>The scaling effects are discussed in the revised vision in lines 207-215, page 11. The Froude number in our experiment ranged from 1.14 to 1.16. It meant that the debris flows in the experiments were supercritical flow (in lines 91-92, page 5).</p>
<p><b>12.</b> I miss a sensitivity study on different debris-flow mixtures (e.g. higher densities, water content variations)</p>	<p>The variation of debris-flow density (different debris-flow mixtures) on scour depth was added in lines 135-141, page 7.</p>
<p><b>13.</b> I miss information on the LRF. What is the sampling rate (in Hz) of the device? How are</p>	<p>The information on the LRF was given in lines 89-90, page 5 and the sampling rate</p>

splashing effects handled?	(Frequency) was added in line 90, page 5.
<p><b>14.</b> What would happen, if there is driftwood involved? Did you test that or what do you expect in such a case?</p>	<p>Debris flows with driftwood will speed up the blockage and jamming of a check dam. Provided that driftwood is involved in our experiments, the check dam will capture driftwood when it passed through the spillway with debris flows. The subsequent debris flows will overflow from the check dam crest once the spillway is blocked by the driftwood, which will cause scour downriver of a check dam. The debris flows with driftwood was not considered in the current experiments, but definitely the reviewer has raised a very important question. The related experiments will be carried out to investigate the behaviour of debris flows with driftwood and its scour feature in the future.</p>
<p><b>15.</b> Can you say something about abrasion rates and the expected life time of such structures?</p>	<p>Abrasion occurs due to the interaction between solid particles in debris flows and the boundary of hydraulic structures. For a spillway with curved bottom, the reaction of centrifugal force exerting on spillway bottom enhance the interaction between the solid particles and the bottom (a component of the reaction force has the same direction as the gravitational force of debris flows near the outlet of the spillway). Although abrasion phenomenon is common, it is difficult to quantify the abrasion rate during an episode of debris flows.</p> <p>Abrasion may be one of the factors lead to the</p>

	<p>damage of spillway with lateral contraction. However, some methods can be taken to mitigate the abrasion damage of such structures by using anti-abrasion materials, or add the protecting layer. The check dam with lateral contracted spillway, like other check dams, the expected life time mainly depends on the debris-flow scales, flow velocity, particle concentration, etc.</p>
--	--

# Effects of Y-type spillway lateral contraction ratios on debris flow patterns and scour features ~~downriver of a check dam~~behind a check dam

Huayong Chen<sup>1,2</sup>, Jinfeng Liu<sup>1,2</sup>, and Wanyu Zhao<sup>1,2</sup>

<sup>1</sup>Key Laboratory of Mountain Hazards and Earth Surface Process Chinese Academy of Sciences (CAS), Chengdu 610041, China

<sup>2</sup>Institute of Mountain Hazards and Environment, CAS, Chengdu 610041, China

*Correspondence to:* Huayong Chen (hychen@imde.ac.cn)

**Abstract.** Debris flows often cause devastating damage to property and can injure or kill residents in mountainous areas. The construction of check dams in ~~debris-debris-flow~~ valleys is considered a useful strategy for mitigating the damages downstream. In this paper, a new type of spillway structure with lateral contraction was proposed to distribute debris flows after the check dam storage filled up. Four different lateral contraction ratios of the spillway were considered in experiments that investigated ~~debris-debris-flow~~ patterns, scour characteristics, and energy dissipation rates when debris flows passed through the spillway. The results indicated that lateral contraction considerably influenced the extension of ~~debris-debris-flow~~ nappes. The drop length of the nappe at  $\eta=0.7$  ( $\eta$  means lateral contraction ratio) was approximately 1.4 times larger than at  $\eta=0.4$ . The collision, friction, and mixing forces between the ~~debris-debris-flow~~ nappes and debris flows in downstream plunge pools dissipated much of the ~~debris-debris-flow~~ kinetic energy, ranging from 42.03% to 78.08% at different contraction ratios. Additionally, based on a dimensionless analysis, an empirical model was proposed to predict the maximum scour depth ~~behind the check dam~~downriver of a check dam. It indicated that the results calculated by the model exhibited good agreement with the experimental results.

## 1 Introduction

Debris flows are formed by poorly sorted, water-saturated materials that mobilize in upstream regions of valleys and surge down slopes in response to gravitational attraction (Iverson, 1997). Large scale debris flows were triggered by intensive rainfalls after the “5.12” Wenchuan Earthquake, including the Zhouqu debris flow,

24 the Wenjia gully debris flow, and the Hongchun gully debris flow (Wang, 2013; Yu et al. , 2013; Tang et al.,  
25 2015). On August 8, 2010, a large debris flow occurred in the Luojiayu gully, northern Zhouqu County, Gansu  
26 Province. The flow destroyed six villages, blocked the Bailongjiang River, resulting in the formation of a lake  
27 that inundated over half of Zhouqu County, and displaced or killed 1765 people (Cui et al., 2013). Usually,  
28 large-scale debris flow events involve substantial erosion upstream (Ni et al., 2012; Yu et al., 2013), and large  
29 volumes of solid materials are transported from the initiation zone~~formation region~~ to downstream areas ~~by~~  
30 ~~debris flows~~.

31 The construction of check dams is considered one of the most effective ways to store solid materials and  
32 control soil erosion in a valley. This structural counter-measure is commonly used to stabilize bank slopes,  
33 flatten the gradients of valleys, reduce flow velocity, and decrease the peak-discharge of debris flows (Lenzi,  
34 2002; Mizuyama, 2008; Remaître et al., 2008; Remaitre and Malet, 2010). Two main types of check dams are  
35 applied to control debris flows (i.e., closed-type and opened-type). Opened-type dams trap boulders, cobble, and  
36 gravel, allowing small particles, fine sediments, and water to pass through the dams (Abedini et al., 2012).  
37 Closed-type dams not only trap the coarse particles but also retain most small particle materials (Heumader,  
38 2000; Lien, 2003). Generally, the dam storage volume of a closed-type check dam is quickly filled with ~~debris~~  
39 ~~debris~~-flow material when a large debris flow occurs. The sequent debris flows directly overflow the check dam,  
40 which can lead to serious scour on and around the foundation of the check dam (Figure 1).

41 Flow patterns and scour caused by the discharge of clear water or sediment flows has been well studied in  
42 hydraulic engineering. The characteristics of free-falling nappes behind the spillway of a gravity dam were  
43 investigated and the drop length of the free jet was predicted based on the energy equation in which the energy  
44 dissipation was neglected at two chosen cross-section (Toombes et al., 2008). Experimental investigations of  
45 aeration associated with overflow dams with curved surfaces were carried out, and empirical correlations

46 predicting the aeration efficiencies of these differently shaped spillways were developed (Chu et al., 2014). An  
47 interpolation formula for predicting scour depth was proposed based on experimental data. It indicated that the  
48 maximum scour increased with increasing discharge and decreased with increasing downstream tail water depth  
49 (Adduce et al., 2005). In addition to the discharge and downstream tail water depth, the characteristic grain size  
50 and the plunge angle were also considered for scour depth prediction (Bormann and Julien, 1991). Considerable  
51 attention has been given to the flow patterns and scour caused by clear flows or sediment flows behind dams.  
52 However, few studies have investigated the ~~debris-debris~~-flow patterns and scour features behind check dams  
53 (Pan et al., 2013), especially for spillway structures with lateral contraction. The flow patterns and scour features  
54 caused by debris flows are different from those caused by clear water or sediment flows due to different flow  
55 densities, cohesion, and particle volume concentrations. The investigation on characteristics of debris flows  
56 discharging and scouring with the new spillway (Y-type spillway) can ~~help us better understand the enrich our~~  
57 ~~knowledge of scour control for debris-flow mitigation.interaction between debris flows and the erodible solid~~  
58 ~~materials, which can also help us to find out better methods for debris flow mitigation in some serious geology~~  
59 ~~conditions.~~  
60 In this paper, a new spillway structure with lateral contraction ~~was-is~~ proposed. Experiments with different  
61 spillway contraction ratios were conducted to study the characteristics of ~~debris-debris~~-flow nappes and scour  
62 after debris flows overflowed the check dam. For each experimental test, video cameras were used to record the  
63 trajectories of ~~debris-debris~~-flow nappes. The energy dissipation rate was analyzed due to the varying lateral  
64 contraction ratios. Finally, an empirical model based on dimensionless analysis was proposed to predict the  
65 maximum scour depth ~~behind the check damdownriver of a check dam.~~

## 66 **2 Experimental setup**

67 The experiments were performed at the Dongchuan Debris Flow Observation and Research Station (DDFORS)

68 in Dongchuan District, Yunnan Province, China. Generally, the experimental flume consisted of a hopper, a gate,  
69 a rectangular channel, and the downstream erodible bed (Figure 2a). The rectangular channel was approximately  
70 4.0 m long, 0.4 m wide, and 0.4 m high, with a slope of  $8^\circ$  (Figure 2b). A check dam made of steel material was  
71 located at the end of the rectangular channel. The shape of the spillway inlet was a 0.20 m wide by 0.10 m high  
72 rectangle. The outlet was shaped like a capital letter 'Y'. The top width of the outlet was equal to that of the inlet.  
73 The bottom width ranged from 0.06 m to 0.12 m due to the different contraction ratios of the spillway. The  
74 dimensions of the spillway are shown in Figure 2c.

75 The lateral contraction ratio  $\eta$  is defined as follows:

$$\eta = \frac{B-b}{B} \quad (1)$$

76 where  $B$  is the width of the spillway inlet and  $b$  is the width of the spillway outlet. When  $b=B$ ,  $\eta=0$ .

77 The storage of the check dam was filled with the solid materials from Jiangjia ravine, with a slope of  $3^\circ$ . The  
78 diameter of the solid material was smaller than 20.0 mm. Its particle size distribution is shown in Fig. 3. Particle  
79 size distribution may affect the ~~debris-debris~~-flow density and flow motion along the channel. The solid  
80 materials used in this experiment was prepared according to the sample of typical debris flows and excluded  
81 particles larger than 20.0 mm due to the limitations of the experimental conditions. The diameter of the solid  
82 materials in the erodible bed was also smaller than 20.0 mm. In addition, the clay and fine particles (smaller than  
83 1.0 mm) were excluded to avoid the effects of matric suction on the development of the scour hole. The particle  
84 size distribution of the erodible bed materials is also shown in Figure 3.

85 In each experimental test, a laser range finder (LRF) was set at the end of the erodible bed to monitor the  
86 depth of the debris flow during the entire process, as shown in Figure 4. The LRF measured the distance  
87 between the original bottom and the laser receiver. When debris flows flowed over the channel bottom, the  
88 LRF measured the distance between the ~~debris-debris~~-flow surface and the laser receiver. The distance



89 difference was the flow depth. The measurement range of the LRF was up to 30.0 m, with an accuracy of  
90  $\pm 0.001$  m. The sampling frequency of the LRF was about 31.0 Hz. The elevation difference between the initial  
91 position and the flow surface was the measured flow depth. The Froude number in our experiment ranged from  
92 1.14 to 1.16. It meant that the debris flows in the experiments were supercritical flow. An example of the  
93 measured results is shown in Figure 5. It reveals that although the ~~debris-debris~~-flow process is not steady over  
94 time, the debris flow over a short period can be considered steady flow. Therefore, the energy conservation  
95 equation derived based on the steady flow assumption can be applied to analyze the energy dissipation rate of a  
96 debris flow.

### 97 **3 Experimental results and analysis**

#### 98 **4.1 Flow patterns of different contraction ratios**

99 When debris flows overflowed the spillway with a high lateral contraction ratio ( $\eta=0.7$ ), the flow depth and  
100 velocity increased dramatically. The ~~debris-debris~~-flow nappe clearly extended in the flow direction.  
101 Furthermore, the debris flows near both side wall, which were forced to change direction by the walls, collided  
102 at the outlet when the debris flows overflowed from the spillway (Figure 6a). Decreasing the lateral contraction  
103 ratio caused the flow depth and velocity to decrease at the same flow discharge. Therefore, the drop length of the  
104 ~~debris-debris~~-flow nappe decreased in the flow direction. The drop length at  $\eta=0.7$  was approximately 1.4 times  
105 than at  $\eta=0.4$  (Table 1). Lateral contraction not only affected the drop length but also broadened the nappe width  
106 due to the collision of debris flows at the outlet (Figure 6b-d). When  $\eta=0.5$ , the broadening ratio  $\kappa$  ( $\kappa$  is the ratio  
107 of nappe width to the outlet width) reached its maximum value ( $\kappa=2.93$  in Table 1). The nappe width was equal  
108 to that of the spillway ( $\kappa=1.0$ ) when there was no lateral contraction at the spillway.

109 If debris flows flowing out of the spillway are considered free-motion point masses under the influence of  
110 gravity, the trajectory of a ~~debris-debris~~-flow nappe can be expressed as follows (Figure 7):

111 
$$y = xtg\varphi + \frac{g}{2v_1^2 \cos^2 \varphi} x^2 \quad (2)$$

$$x = \frac{v^2}{g} \cos \varphi \left( \sqrt{\sin^2 \varphi + \frac{2gy}{v^2}} - \sin \varphi \right) \varphi \geq 0 \quad (3)$$

112 When  $\varphi = 0$ , equation (2) simplifies to equation (3):

$$x = \sqrt{\frac{2v^2 y}{g}} \quad (4)$$

113 where  $v$  is the initial velocity of the debris flow flowing out of the spillway,  $\varphi$  represents the angle of the  
114 initial velocity in the horizontal direction, and  $y$  is the water elevation difference.

115 Equation (3) indicates that the nappe extension in the horizontal direction 'x' is proportional to the initial  
116 velocity  $v$  and square root of the water elevation difference  $y$ . From Fig. 6 and Table 1, we found that when  
117  $\eta=0.7$ , the nappe extension was longest in the flow direction. From this point of view, a high lateral contraction  
118 ratio increased the distance between the plunge point and the dam toe, which effectively protected the dam  
119 foundation from scouring. The hydraulic characteristics of the nappe away from the spillway at different lateral  
120 contraction ratios were shown in Figure 8 and Figure 9. Figure 8 indicates that increasing the lateral contraction  
121 ratio decreased the width of the ~~debris-debris~~-flow nappe. Furthermore, the higher lateral contraction of the  
122 spillway strengthened the collision between flows at the spillway outlet. Air bubbles were entrained in the debris  
123 flows when the continuum of the debris flows was broken. Figure 9 shows the extent of the ~~debris-debris~~-flow  
124 nappes. The distribution of the flow velocity in the vertical direction at the outlet increased with increasing flow  
125 depth due to the effects of boundary friction. Therefore, the longest flow nappes were formed by the debris flows  
126 with relatively large velocities at the flow surface.

127 **4.2 Debris-flow scour features ~~behind the check dam~~downriver of a check dam**

128 The scour features of debris flows ~~behind the check dam~~downriver of a check dam represent one of the most

129 important indexes, which determines the scour depth at the dam foundation. Figure 10 shows the effects of  
130 lateral contraction on the formation of scour holes in an erodible bed. For the same curvature of the spillway  
131 surface, decreasing the contraction ratio decreased the maximum scour depth and caused the location of the  
132 maximum scour point to shift toward the dam toe due to the decreased ~~debris-debris~~-flow velocity. The  
133 maximum scour depth and its location farther from the dam toe for  $\eta=0.7$  were approximately 1.3 and 1.4 times,  
134 respectively, larger than for  $\eta=0.4$ . Although a high lateral contraction ratio extended the ~~debris-debris~~-flow  
135 nappe, it also increased the scour depth in the erodible bed to some extent. In addition, debris-flow density has  
136 some effects on the scour depth. Figure 11 indicates the scour depth caused by debris flow with density of  
137 1200kg/m<sup>3</sup> is a bit larger than that caused by debris flow with density of 1500kg/ m<sup>3</sup> at a certain lateral  
138 contraction ratio (Figure 11). It was explained that the debris flow with lower particle concentration (Lower  
139 debris-flow density) initialized and carried more bed materials than that with higher particle concentration  
140 (Higher debris-flow density) when the other factors were fixed (Such as longitudinal slope of gully, debris-flow  
141 scale, lateral contraction ratio of the spillway).

#### 142 4.3 Energy dissipation at different contraction ratios

143 Generally, different energy dissipaters such as the plunge pool (Pagliara et al., 2010; Duarte et al., 2015) or  
144 step-pool systems (Yu, 2007; Wang et al., 2009; Wang et al., 2012) are required to dissipate the kinetic energy of  
145 the surplus flow and prevent the dam foundation and riverbed from scouring when sudden changes to the  
146 channel slope occur. The energy dissipation process of the check dam was estimated using the Bernoulli equation  
147 (4). The rationale behind using this equation was previously mentioned.

148 The Bernoulli equation between two reference cross-sections is written as follows:

$$Z_1 + h_1 + \alpha_1 \frac{v_1^2}{2g} = Z_2 + h_2 + \alpha_2 \frac{v_2^2}{2g} + h_w \quad (5)$$

149 If  $\Delta Z = Z_1 - Z_2$ , then equation (4) can be transformed into equation (5):

$$\Delta Z + h_1 + \alpha_1 \frac{v_1^2}{2g} = h_2 + \alpha_2 \frac{v_2^2}{2g} + h_w \quad (6)$$

150 The energy dissipation coefficient  $\zeta$  can be expressed as follows:

$$\zeta = 1 - \frac{h_2 + \frac{v_2^2}{2g}}{\Delta Z + h_1 + \frac{v_1^2}{2g}} \quad (7)$$

151 where  $Z_1$  and  $Z_2$  are the elevations of reference cross-sections #1 and #2 (Figure. 2b), respectively;  $h_1$  and  $h_2$   
152 are the depths of debris flows at reference cross-sections #1 and #2, respectively;  $v_1$  and  $v_2$  are the velocities of  
153 the debris flows at references cross-sections #1 and #2, respectively;  $\alpha_1$  and  $\alpha_2$  are the kinetic energy correction  
154 coefficients ( $\alpha_1=\alpha_2=1$ ) (Adamkowski et al., 2006);  $\Delta Z$  is the elevation difference between the two reference  
155 cross-sections; and  $h_w$  is the water head loss.

156 Table 2 indicates that the collision and friction forces between the ~~debris-debris~~-flow nappes and debris flows  
157 in the plunge pool dissipated the kinetic energy of the flows, ranging from 42.03% to 78.08% at different  
158 contraction ratios. In the case of  $V=0.16 \text{ m}^3$ , the energy dissipation rate decreased gradually when the contraction  
159 ratio changed from 0.7 to 0.4 because the high contraction ratio increased the number of ~~debris-debris~~-flow  
160 collisions when it passed through the spillway. In the cases of  $V=0.10 \text{ m}^3$  and  $V=0.06 \text{ m}^3$ , the energy dissipation  
161 rate also decreased with decreasing the contraction ratios except at  $\eta=0.4$ . The mean value of the energy  
162 dissipation rate demonstrated a good positive correlation between the energy dissipation rate and the lateral  
163 contraction ratio. In addition, for the same contraction ratio, the energy dissipation rate increased gradually with  
164 decreasing ~~debris-debris~~-flow scale.

#### 165 4.4 The empirical equation for estimating the maximum scour depth

166 Many empirical equations have been proposed to predict the maximum scour depth over the last several

167 decades (Bormann and Julien, 1991; Zhou, 1991; Adduce et al., 2005; Pan et al., 2013). The main parameters  
 168 include the unit discharge, characteristic particle size of the erodible bed, water elevation difference and clear  
 169 water and ~~debris-debris~~-flow densities. However, most of the empirical equations (Li and Liu, 2010) neglect  
 170 dimensional homogeneity (the empirical equations should be dimensionally homogeneous). For new type of  
 171 spillway, the lateral contraction ratio is an important parameter for predicting the maximum scour depth. For a  
 172 debris flow, the maximum scour depth is mainly determined by the following parameters:

$$h_d = f(q, g, \rho_d, \rho_w, d_{90}, \eta, \dots) \quad (8)$$

173 where  $h_d$  is the maximum scour depth,  $q$  is the unit discharge of the debris flow,  $g$  is the acceleration due to  
 174 gravity,  $\rho_d$  and  $\rho_w$  are the ~~debris-debris~~-flow density and clear water density, respectively (two ~~debris-debris~~-flow  
 175 densities were considered, including  $\rho_d=1200\text{kg/m}^3$  and  $\rho_d=1500\text{kg/m}^3$ ),  $d_{90}$  is the characteristic particle size for  
 176 erodible bed materials, and  $\eta$  is the lateral contraction ratio.

177 Based on a dimensional analysis, the dimensionless parameters with clear physical meanings are developed as  
 178 follows:

$$\frac{h_s}{d_{90}} = k \left( \frac{q}{d_{90} \sqrt{g d_{90}}} \right)^{a_1} \left( \frac{\rho_d}{\rho_w} \right)^{a_2} (1-\eta)^{a_3} \quad (9)$$

179 where  $h_s/d_{90}$  is dimensionless scour depth,  $k$  is a coefficient,  $a_i$  is an index ( $i=1, 2, 3$ ),  $\frac{q}{d_{90} \sqrt{g d_{90}}}$  is the  
 180 dimensionless discharge, and  $\rho_d/\rho_w$  is the dimensionless density.

181 According to the experimental data, the regression equation can be expressed as follows:

$$\frac{h_s}{d_{90}} = 3.15 \left( \frac{q}{d_{90} \sqrt{g d_{90}}} \right)^{0.51} \left( \frac{\rho_d}{\rho_w} \right)^{-0.1363} (1-\eta)^{0.7583} \quad (10)$$

182 The regression equation suggests that the flow density had relatively small effects on the depth of the scour  
 183 hole. However, the ~~debris-debris~~-flow discharge and the lateral contraction had strong effects on the maximum  
 184 depth of the scour hole, which directly determined the kinetic energy of the flow in the downstream erodible bed.

185 The validation tests were also performed using the physical experimental model shown in Figure 2, but under  
186 different conditions. Additional experimental data provided in the literature (Ben and Mossa, 2006) were used to  
187 verify the reliability of the regression equation. The predicted results exhibited good agreement with the  
188 experimental results. The absolute error was smaller than 15.0% in most cases, as shown in Figure ~~4~~12.

## 189 **4 Conclusions and Discussions**

### 190 **4.1 Conclusions**

191 The characteristics of debris flows overflowing the new type of spillway were analyzed at different lateral  
192 contraction ratios. The energy dissipation rate and an empirical model for predicting the maximum scour depth  
193 were also studied in this paper. The following conclusions were drawn from this analysis:

194 1) Flow patterns were mainly determined by the lateral contraction ratio. At a high lateral contraction ratio, the  
195 spillway effectively extended the ~~debris-debris~~-flow nappe and increased the distance between the plunge  
196 point and the dam toe. The drop length of the nappe at  $\eta=0.7$  was approximately 1.4 times higher than that  
197 at  $\eta=0.4$ .

198 2) The plunge pool ~~behind the check dam~~downriver of a check dam inevitably dissipated the kinetic energy of  
199 the debris flow after overflowing the check dam. The collision and friction between the ~~debris-debris~~-flow  
200 nappe and the debris flow in the plunge pool dissipated the kinetic energy of the flow, ranging from 42.03%  
201 to 78.08% at different contraction ratios. Generally, increasing the contraction ratio increased the energy  
202 dissipation rate at the same ~~debris-debris~~-flow scale.

203 3) An empirical model was proposed to predict the maximum scour depth ~~behind the check dam~~downriver of  
204 a check dam. The results indicated that the predicted results exhibited good agreement with the  
205 experimental results. The absolute error was smaller than 15.0% in most cases.

### 206 **4.2 Discussions**

207 The characteristics of debris flow nappe and scour downriver of a check dam with different spillway were

208 experimentally investigated in this article. When the experimental data are used to predict debris-flow motion  
209 and scour feature downriver of a check dam in prototype, the effects of physical model scale should be  
210 considered. Scaling effect is mainly induced by dissatisfaction of mobility similitude of model sediment in  
211 physical model experiments and it leads to discrepancies between the estimated and actual scour results. Just like  
212 the experimental investigation on the scale effect in pier-scour experiments, the bed-particle mobility similitude  
213 (Ettema et al., 1998; Ettema and Melville, 1999) or the flow-strength similitude (Lee and Sturm, 2009) should be  
214 satisfied to weaken or eliminate the scaling effect for debris-flow scour when the experimental results are  
215 extrapolated to predict prototype performance in the future.

216 When debris flows occur in the mountainous areas with forest the driftwood carried by debris flows is a  
217 common phenomenon. The debris flows combined with driftwood will speed up blockage and jamming of a  
218 check dam. Once the spillway is blocked by the driftwood the subsequent debris flows will overflow from the  
219 crest of a check dam, which will cause extensive scour downriver of a check dam. Therefore, it is also necessary  
220 to investigate the behavior of debris flows with driftwood and propose some reasonable structural or non-  
221 structural countermeasures to mitigate the effects of debris flows with driftwood on the operation of a check dam  
222 in the future.

## 223 **Acknowledgments**

224 The study results presented in this paper were supported by the Key Research Program of the Chinese  
225 Academy of Sciences (Grant No. KZZD-EW-05-01), the National Natural Science Foundation of China (Grant  
226 No.51209195), the Science Technology Service Network Initiative, Chinese Academy of Sciences (Grant No.  
227 KFJ-EW-ST-094), and the Key Laboratory of Mountain Hazards and Earth Surface Process, Chinese Academy  
228 of Sciences.

## 229 **List of symbols**

- $a_i$  = The index for the dimensionless parameter (-)
- $b$  = The width of the spillway outlet(m)
- $B$  = The width of the spillway inlet (m)
- $d_{90}$  = The characteristic particle size for erodible bed materials (m)
- $k$  = The coefficient for the dimensionless equation (-)
- $h_1$  = The depth of debris flows at reference cross-sections #1 (m)
- $h_2$  = The depth of debris flows at reference cross-sections #2 (m)
- $h_d$  = The maximum scour depth (m)
- $h_w$  = The water head loss (m)
- $g$  = The acceleration of gravity ( $m/s^2$ )
- $q$  = The unit discharge of the debris flow ( $m^3/s$ )
- $v$  = The initial velocity of the debris flow flowing out of the spillway(m/s)
- $v_1$  = The velocity of debris flows at reference cross-sections #1 (m/s)
- $v_2$  = The velocity of debris flows at reference cross-sections #2 (m/s)
- $V$  = The scale of debris flow in the experiments ( $m^3$ )
- $x$  = Trajectory in the horizontal direction (m)
- $y$  = The water elevation difference (m)
- $Z_1$  = The elevation of reference cross-sections at #1 (m)
- $Z_2$  = The elevation of reference cross-sections at #2 (m)
- $\Delta z$  = The elevation difference between the two reference cross-sections (m)

Greek letters

- $\alpha_1$  = The kinetic energy correction coefficient for  $v_1$  (-)
- $\alpha_2$  = The kinetic energy correction coefficient for  $v_2$  (-)
- $\rho_d$  = The density of debris flows ( $kg/m^3$ )
- $\rho_w$  = The density of clear water ( $kg/m^3$ )
- $\zeta$  = The energy dissipation coefficient(-)
- $\eta$  = The lateral contraction ratio(-)
- $\varphi$  = The angle of the initial velocity in the horizontal direction( $^\circ$ )

230

231



232       **References**

- 233       Abedini, M., Said, M. A. M., and Ahmad, F.. Effectiveness of check dam to control soil erosion in a tropical  
234           catchment (The Ulu Kinta Basin), *Catena*, 97, 63-70, 2012.
- 235       Adamkowski, A., Janicki, W., Kubiak, J. et al.: Water turbine efficiency measurements using the gibson method  
236           based on special instrumentation installed inside pipelines//Proceedings of the 6th International Conference  
237           on Innovation in Hydraulic Efficiency Measurements, 2006.
- 238       Adduce, C., La Rocca, M., and Sciortino, G.: Local Scour Downstream of Grade Control Structures in Urban  
239           Stream Restoration, Enhancing Urban Environment by Environmental Upgrading and Restoration Nato  
240           Science Series IV: Earth and Environmental Sciences, 43, 307-317, 2005.
- 241       Ben Meftah, M., and Mossa, M.: Scour holes downstream of bed sills in low-gradient channels, *J. Hydraul. Res.*,  
242           44,497-509, 2006.
- 243       Bormann, E., and Julien, P.Y.: Scour Downstream of Grade-control Structures, *J. Hydraul. Eng.*, 117(5), 579-594,  
244           1991.
- 245       Chu, K.J., Hua, Z.L., and Ji, L.J.: Aeration at overflow dams with curved surfaces by different flashboard  
246           spillways, *J. Environ. Eng. Landsc.*, 22(3), 226-236, 2014.
- 247       Cui, P., Zhou, Gordon G.D., Zhu, X.H., and Zhang, J.Q.: Scale amplification of natural debris flows caused by  
248           cascading landslide dam failures, *Geomorphology*, 182,173-189, 2013.
- 249       Duarte, R., Schleiss, A. J., and Pinheiro, A.: Influence of jet aeration on pressures around a block embedded in a  
250           plunge pool bottom, *Environ Fluid Mech.*, 15(3), 673-693, 2015.
- 251       [Ettema, R., Melville, B. W., Barkdoll, B.: Scale effect in pier-Scour experiments, J Hydraul Eng-ASCE.,](#)  
252           [124\(6\):639-642, 1998.](#)
- 253       Heumader, J.: Technical debris-flow countermeasures in Austria—a review, *Proceedings, Second International*

254 Conference on Debris-Flow Hazards Mitigation: Mechanics, Prediction, and Assessment, 553-564, 2000.

255 Iverson, R. M.: The physics of debris flows, *Rev. Geophys.*, 35(3), 245-296, 1997.

256 [Laursen, E. M.: Scale effect in pier-scour experiments, \*J Hydraul Eng-ASCE.\*, 125\(8\):894-895, 1999.](#)

257 [Lee, S. O., Sturm, T. W.: Effect of Sediment Size Scaling on Physical Modeling of Bridge Pier Scour, \*J Hydraul\*](#)

258 [\*Eng-ASCE.\*, 135\(10\):793-802,2009.](#)

259 Lenzi, M. A.: Stream bed stabilization using boulder check dams that mimic step-pool morphology features in

260 Northern Italy, *Geomorphology*, 45(3), 243-260, 2002.

261 Lien, H.P.: Design of Slit Dams for Controlling Stony Debris Flows. *Int J Sediment Res.* ,18(1),74-87, 2003.

262 Mizuyama, T.: Structural countermeasures for debris flow disasters, *International Journal of Erosion Control*

263 *Engineering*, 1(2), 38-43, 2008.

264 Ni, H. Y., Zheng, W. M., and Tie, Y. B.: Formation and characteristics of post-earthquake debris flow: a case

265 study from Wenjia gully in Mianzhu, Sichuan, SW China, *Nat. hazards*, 61(2),317-335, 2012.

266 Pagliara, S., Roy, D., and Palermo, M.: 3D plunge pool scour with protection measures, *J. Hydro-environ Res.*, 4,

267 225-233, 2010.

268 Pan, H.L., Wang, R., Huang, J.C., and Ou, G.Q.: Study on the ultimate depth of scour pit downstream of debris

269 flow check dam based on the energy method, *Eng. Geol.*, 160,103-109, 2013.

270 Remaître, A., Van Asch, T. W. J., and Malet J. P.: Influence of check dams on debris-flow run-out intensity, *Nat.*

271 *Hazard Earth Sys.*, 8(6), 1403-1416, 2008.

272 Remaitre, A., and Malet, J. P.: The effectiveness of torrent check dams to control channel instability: example of

273 debris-flow events in clay shales. Check dams, morphological adjustments and erosion control in torrential

274 streams, Nova Science Publishers Inc., New York, 211-237, 2010.

275 Tang, C., Jiang, Z., and Li, W.: Seismic Landslide Evolution and Debris Flow Development: A Case Study in the

276 Hongchun Catchment, Wenchuan Area of China, *Engineering Geology for Society and Territory*, 2, 445-449,  
277 2015.

278 Toombes, L., Wagner, C., and Chanson, H.: Flow patterns in nappe flow regime down low gradient stepped  
279 chutes, *J. Hydraul Res.*, 46(1), 4-14, 2008.

280 Wang, G. L.: Lessons learned from protective measures associated with the 2010 Zhouqu debris flow disaster in  
281 China, *Nat. Hazards*, 3(69), 1835-1847, 2013.

282 Wang, Z. Y., Melching, C.S., Duan, X.H., and Yu, G.A.: Ecological and hydraulic studies of step-pool systems, *J.*  
283 *Hydraul. Eng.*, 9,705-717, 2009.

284 Wang, Z.Y., Qi, L.J., and Wang, X. Z.: A prototype experiment of debris flow control with energy dissipation  
285 structures, *Nat. Hazards*, 60, 971-989, 2012.

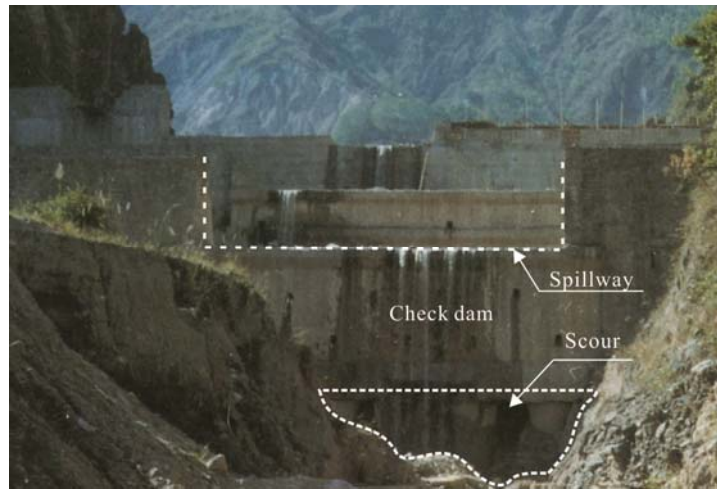
286 Yu, B., Ma, Y., and Wu, Y.: Case study of a giant debris flow in the Wenjia Gully, Sichuan Province, China, *Nat.*  
287 *hazards*, 65, 835-849, 2013.

288 Yu, G.A., Wang, Z.Y., and Duan, X.H.: Artificial step-pool system for ecological restoration of a debris-flow  
289 ravine, In: *Proceedings of 32nd IAHR congress, Venice, Italy*, 1-10, July 2007.

290

291

292  
293

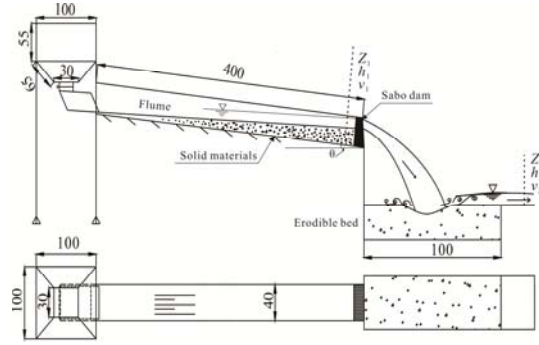


294  
295 |  
296

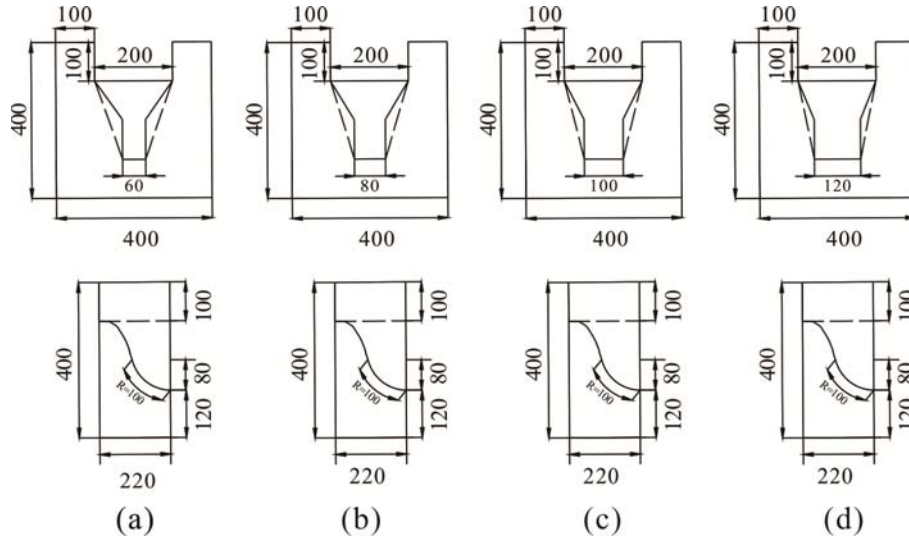
**Fig. 1.** An example of foundation scour downriver of~~behind~~ a check dam



(a) Photograph of the experimental setup



(b) Schematic diagram of the experimental setup (unit: cm)



(a)

(b)

(c)

(d)

298

299

300

301

302

303

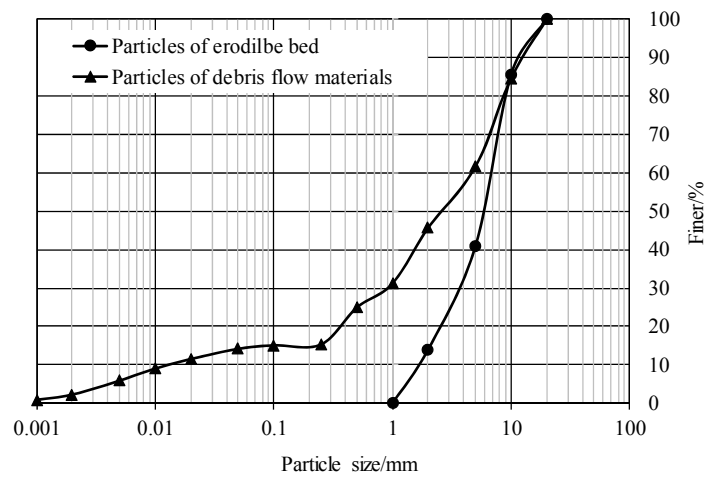
304

305

(c) The structure and dimensions of the spillway (unit: mm). Four different lateral contraction ratios were considered in the experiments: (a)  $B=200.0$  mm,  $b=60.0$  mm,  $\eta=0.7$ ; (b)  $B=200.0$  mm,  $b=80.0$  mm,  $\eta=0.6$ ; (c)  $B=200.0$  mm,  $b=100.0$  mm,  $\eta=0.5$ ; (d)  $B=200.0$  mm,  $b=120.0$  mm,  $\eta=0.4$ . The bottom of the spillway was formed by a compound curve surface (a simple curved segment and a circular segment: radius  $R=100.0$  mm, radius angle  $\delta=75^\circ$ ).

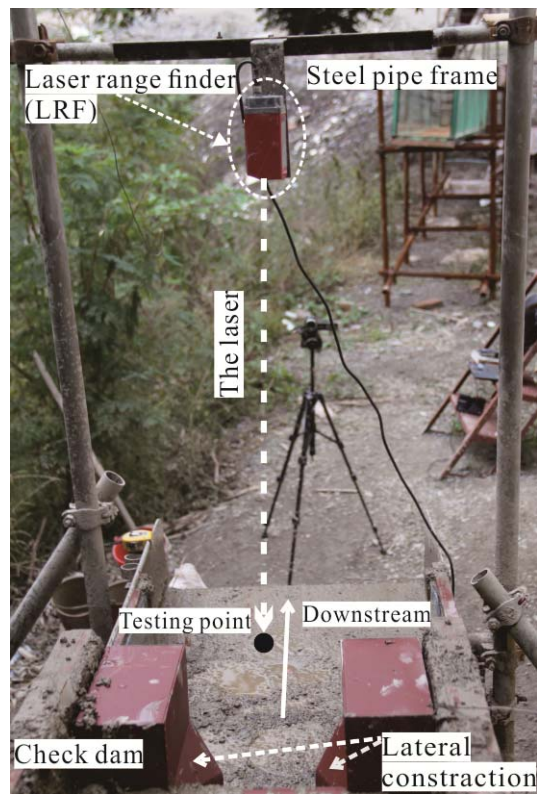
**Fig. 2.** Experimental setup

306  
307



308  
309  
310

**Fig. 3.** The particle size distribution of samples for the debris flows and erodible bed



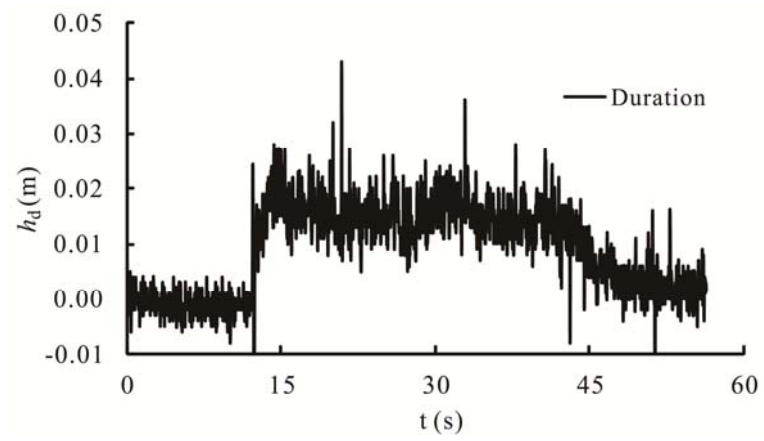
312

313

314

**Fig. 4.** Photograph of the LRF system (the photograph was taken in the downstream direction)

315

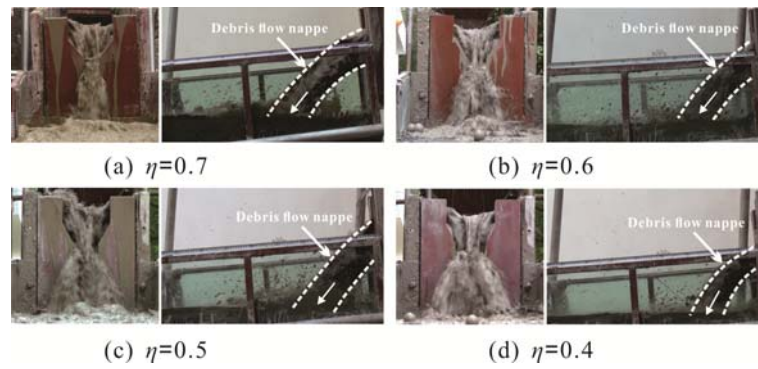


316

317 | **Fig. 5.** An example of a [debris-flow hydrograph](#)-~~debris flow duration~~ monitored by the LRF

318

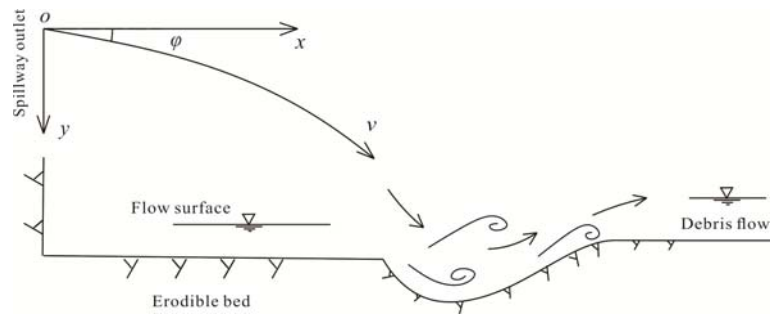




320

321 **Fig. 6.** Various debris flow patterns at different lateral contraction ratios (the pictures on the left were taken  
322 from a downstream view)

323



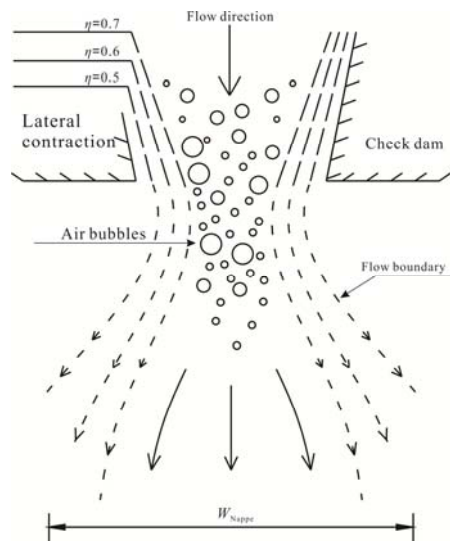
324

325 **Fig. 7.** A diagram of dynamic parameters of debris flows

326

327

328



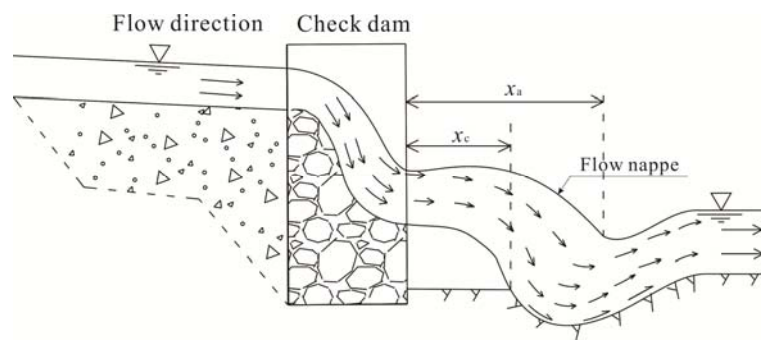
329

330

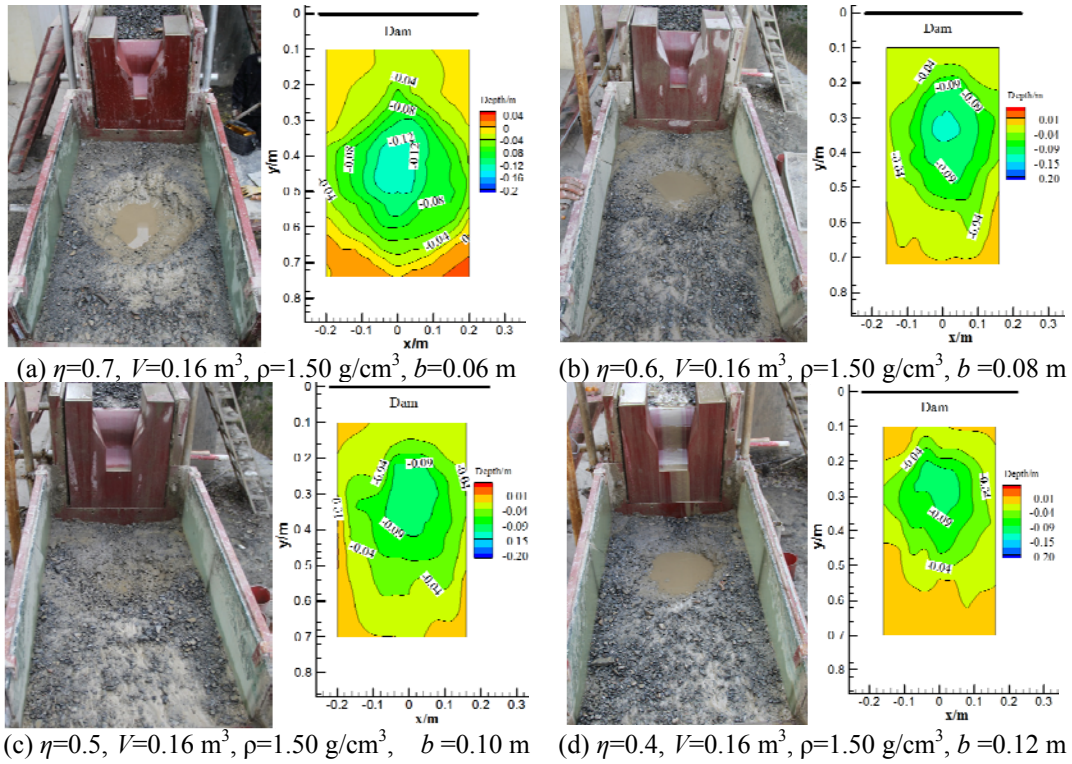
**Fig. 8.** The transverse expansion of a debris flow nappe at different lateral contraction ratios

331

332  
333

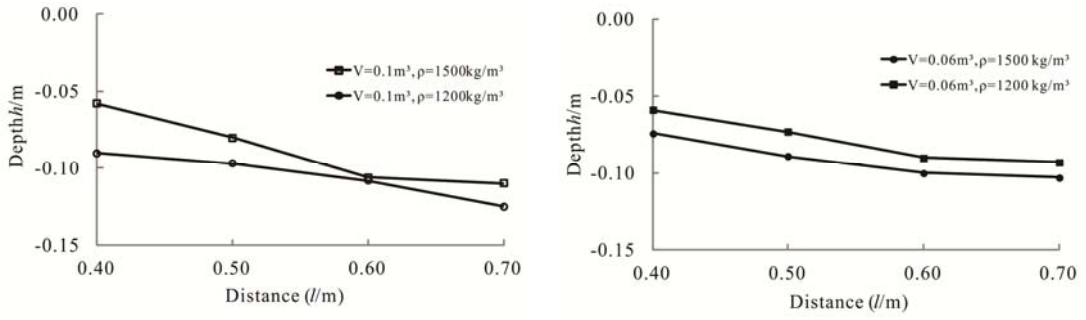


334  
335 **Fig. 9.** The trajectory of a debris flow nappe  
336



338 | **Fig. 10.** The shapes of the scour hole behind the cheek dam downriver of a check dam ( $V=0.16 \text{ m}^3, \rho=1.50 \text{ g/cm}^3$ )  
 339

340  
341



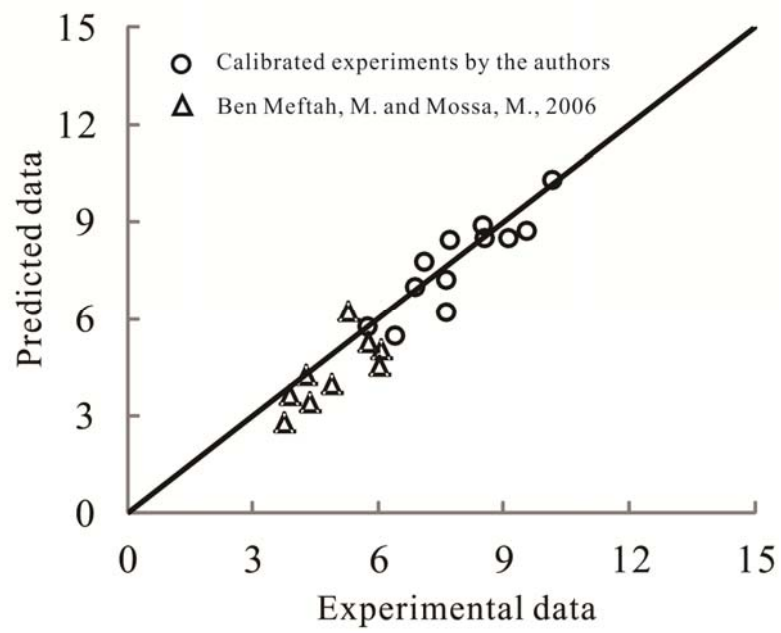
(a)  $V=0.1\text{m}^3$

(b)  $V=0.06\text{m}^3$

**Fig. 11.** Comparison of scour depth at different debris-flow densities

342  
343  
344

345



346

347 | **Fig. 1412.** Comparison between predicted data and experimental ones

348

349 **Table 1.** The main parameters of the debris flow nappe for different contraction ratios

Items	(a)	(b)	(c)	(d)
Width of the outlet $b/\text{mm}$	60.0	80.0	100.0	120.0
Lateral contraction ratio $\eta$	0.7	0.6	0.5	0.4
Width of the nappe $W_{\text{Nappe}}/\text{mm}$	137.2	231.6	292.6	320.6
Broadening ratio $\kappa(\kappa= W_{\text{Nappe}}/b)$	2.29	2.90	2.93	2.67
Length of the nappe away from the outlet $x_a/\text{m}$	0.43	0.34	0.33	0.31
Length of the nappe close to the outlet $x_c/\text{m}$	0.25	0.21	0.21	0.18

350 Notes: B is constant for each spillway type (B =200.0 mm)

351



352 **Table 2.** The energy dissipation rates at different contraction ratios

Scales	Density ( $\rho=1.50 \text{ g/cm}^3$ )			
	$\eta=0.7$	$\eta=0.6$	$\eta=0.5$	$\eta=0.4$
$V=0.16 \text{ m}^3$	66.43%	57.48%	52.34%	42.03%
$V=0.10 \text{ m}^3$	75.37%	72.94%	60.58%	67.97%
$V=0.06 \text{ m}^3$	78.08%	73.70%	63.61%	71.75%
Mean value	73.29%	68.04%	58.84%	60.58%

353

354

355

# Effects of Y-type spillway lateral contraction ratios on debris flow patterns and scour features downriver of a check dam

Huayong Chen<sup>1,2</sup>, Jinfeng Liu<sup>1,2</sup>, and Wanyu Zhao<sup>1,2</sup>

<sup>1</sup>Key Laboratory of Mountain Hazards and Earth Surface Process Chinese Academy of Sciences (CAS), Chengdu 610041, China

<sup>2</sup>Institute of Mountain Hazards and Environment, CAS, Chengdu 610041, China

*Correspondence to:* Huayong Chen (hychen@imde.ac.cn)

**Abstract.** Debris flows often cause devastating damage to property and can injure or kill residents in mountainous areas. The construction of check dams in debris-flow valleys is considered a useful strategy for mitigating the damages downstream. In this paper, a new type of spillway structure with lateral contraction was proposed to distribute debris flows after the check dam storage filled up. Four different lateral contraction ratios of the spillway were considered in experiments that investigated debris-flow patterns, scour characteristics, and energy dissipation rates when debris flows passed through the spillway. The results indicated that lateral contraction considerably influenced the extension of debris-flow nappes. The drop length of the nappe at  $\eta=0.7$  ( $\eta$  means lateral contraction ratio) was approximately 1.4 times larger than at  $\eta=0.4$ . The collision, friction, and mixing forces between the debris-flow nappes and debris flows in downstream plunge pools dissipated much of the debris-flow kinetic energy, ranging from 42.03% to 78.08% at different contraction ratios. Additionally, based on a dimensionless analysis, an empirical model was proposed to predict the maximum scour depth downriver of a check dam. It indicated that the results calculated by the model exhibited good agreement with the experimental results.

## 1 Introduction

Debris flows are formed by poorly sorted, water-saturated materials that mobilize in upstream regions of valleys and surge down slopes in response to gravitational attraction (Iverson,1997). Large scale debris flows were triggered by intensive rainfalls after the “5.12” Wenchuan Earthquake, including the Zhouqu debris flow,

24 the Wenjia gully debris flow, and the Hongchun gully debris flow (Wang, 2013; Yu et al. , 2013; Tang et al.,  
25 2015). On August 8, 2010, a large debris flow occurred in the Luojiayu gully, northern Zhouqu County, Gansu  
26 Province. The flow destroyed six villages, blocked the Bailongjiang River, resulting in the formation of a lake  
27 that inundated over half of Zhouqu County, and displaced or killed 1765 people (Cui et al., 2013). Usually,  
28 large-scale debris flow events involve substantial erosion upstream (Ni et al., 2012; Yu et al., 2013), and large  
29 volumes of solid materials are transported from the initiation zone to downstream areas.

30 The construction of check dams is considered one of the most effective ways to store solid materials and  
31 control soil erosion in a valley. This structural counter-measure is commonly used to stabilize bank slopes,  
32 flatten the gradients of valleys, reduce flow velocity, and decrease the peak-discharge of debris flows (Lenzi,  
33 2002; Mizuyama, 2008; Remaître et al., 2008; Remaitre and Malet, 2010). Two main types of check dams are  
34 applied to control debris flows (i.e., closed-type and opened-type). Opened-type dams trap boulders, cobble, and  
35 gravel, allowing small particles, fine sediments, and water to pass through the dams (Abedini et al., 2012).  
36 Closed-type dams not only trap the coarse particles but also retain most small particle materials (Heumader,  
37 2000; Lien, 2003). Generally, the dam storage volume of a closed-type check dam is quickly filled with  
38 debris-flow material when a large debris flow occurs. The sequent debris flows directly overflow the check dam,  
39 which can lead to serious scour on and around the foundation of the check dam (Figure 1).

40 Flow patterns and scour caused by the discharge of clear water or sediment flows has been well studied in  
41 hydraulic engineering. The characteristics of free-falling nappes behind the spillway of a gravity dam were  
42 investigated and the drop length of the free jet was predicted based on the energy equation in which the energy  
43 dissipation was neglected at two chosen cross-section (Toombes et al., 2008). Experimental investigations of  
44 aeration associated with overflow dams with curved surfaces were carried out, and empirical correlations  
45 predicting the aeration efficiencies of these differently shaped spillways were developed (Chu et al., 2014). An

46 interpolation formula for predicting scour depth was proposed based on experimental data. It indicated that the  
47 maximum scour increased with increasing discharge and decreased with increasing downstream tail water depth  
48 (Adduce et al., 2005). In addition to the discharge and downstream tail water depth, the characteristic grain size  
49 and the plunge angle were also considered for scour depth prediction (Bormann and Julien, 1991). Considerable  
50 attention has been given to the flow patterns and scour caused by clear flows or sediment flows behind dams.  
51 However, few studies have investigated the debris-flow patterns and scour features behind check dams (Pan et al.,  
52 2013), especially for spillway structures with lateral contraction. The flow patterns and scour features caused by  
53 debris flows are different from those caused by clear water or sediment flows due to different flow densities,  
54 cohesion, and particle volume concentrations. The investigation on characteristics of debris flows discharging  
55 and scouring with the new spillway (Y-type spillway) can enrich our knowledge of scour control for debris-flow  
56 mitigation.

57 In this paper, a new spillway structure with lateral contraction is proposed. Experiments with different  
58 spillway contraction ratios were conducted to study the characteristics of debris-flow nappes and scour after  
59 debris flows overflowed the check dam. For each experimental test, video cameras were used to record the  
60 trajectories of debris-flow nappes. The energy dissipation rate was analyzed due to the varying lateral contraction  
61 ratios. Finally, an empirical model based on dimensionless analysis was proposed to predict the maximum scour  
62 depth downriver of a check dam.

## 63 **2 Experimental setup**

64 The experiments were performed at the Dongchuan Debris Flow Observation and Research Station (DDFORS)  
65 in Dongchuan District, Yunnan Province, China. Generally, the experimental flume consisted of a hopper, a gate,  
66 a rectangular channel, and the downstream erodible bed (Figure 2a). The rectangular channel was approximately  
67 4.0 m long, 0.4 m wide, and 0.4 m high, with a slope of  $8^\circ$  (Figure 2b). A check dam made of steel material was

68 located at the end of the rectangular channel. The shape of the spillway inlet was a 0.20 m wide by 0.10 m high  
69 rectangle. The outlet was shaped like a capital letter 'Y'. The top width of the outlet was equal to that of the inlet.  
70 The bottom width ranged from 0.06 m to 0.12 m due to the different contraction ratios of the spillway. The  
71 dimensions of the spillway are shown in Figure 2c.

72 The lateral contraction ratio  $\eta$  is defined as follows:

$$\eta = \frac{B-b}{B} \quad (1)$$

73 where  $B$  is the width of the spillway inlet and  $b$  is the width of the spillway outlet. When  $b=B$ ,  $\eta=0$ .

74 The storage of the check dam was filled with the solid materials from Jiangjia ravine, with a slope of  $3^\circ$ . The  
75 diameter of the solid material was smaller than 20.0 mm. Its particle size distribution is shown in Fig. 3. Particle  
76 size distribution may affect the debris-flow density and flow motion along the channel. The solid materials used  
77 in this experiment was prepared according to the sample of typical debris flows and excluded particles larger  
78 than 20.0 mm due to the limitations of the experimental conditions. The diameter of the solid materials in the  
79 erodible bed was also smaller than 20.0 mm. In addition, the clay and fine particles (smaller than 1.0 mm) were  
80 excluded to avoid the effects of matric suction on the development of the scour hole. The particle size  
81 distribution of the erodible bed materials is also shown in Figure 3.

82 In each experimental test, a laser range finder (LRF) was set at the end of the erodible bed to monitor the  
83 depth of the debris flow during the entire process, as shown in Figure 4. The LRF measured the distance  
84 between the original bottom and the laser receiver. When debris flows flowed over the channel bottom, the  
85 LRF measured the distance between the debris-flow surface and the laser receiver. The distance difference  
86 was the flow depth. The measurement range of the LRF was up to 30.0 m, with an accuracy of  $\pm 0.001$  m. The  
87 sampling frequency of the LRF was about 31.0 Hz. The elevation difference between the initial position and the  
88 flow surface was the measured flow depth. The Froude number in our experiment ranged from 1.14 to 1.16. It

89 meant that the debris flows in the experiments were supercritical flow. An example of the measured results is  
 90 shown in Figure 5. It reveals that although the debris-flow process is not steady over time, the debris flow over a  
 91 short period can be considered steady flow. Therefore, the energy conservation equation derived based on the  
 92 steady flow assumption can be applied to analyze the energy dissipation rate of a debris flow.

### 93 3 Experimental results and analysis

#### 94 4.1 Flow patterns of different contraction ratios

95 When debris flows overflowed the spillway with a high lateral contraction ratio ( $\eta=0.7$ ), the flow depth and  
 96 velocity increased dramatically. The debris-flow nappe clearly extended in the flow direction. Furthermore, the  
 97 debris flows near both side wall, which were forced to change direction by the walls, collided at the outlet when  
 98 the debris flows overflowed from the spillway (Figure 6a). Decreasing the lateral contraction ratio caused the  
 99 flow depth and velocity to decrease at the same flow discharge. Therefore, the drop length of the debris-flow  
 100 nappe decreased in the flow direction. The drop length at  $\eta=0.7$  was approximately 1.4 times than at  $\eta=0.4$   
 101 (Table 1). Lateral contraction not only affected the drop length but also broadened the nappe width due to the  
 102 collision of debris flows at the outlet (Figure 6b-d). When  $\eta=0.5$ , the broadening ratio  $\kappa$  ( $\kappa$  is the ratio of nappe  
 103 width to the outlet width) reached its maximum value ( $\kappa=2.93$  in Table 1). The nappe width was equal to that of  
 104 the spillway ( $\kappa=1.0$ ) when there was no lateral contraction at the spillway.

105 If debris flows flowing out of the spillway are considered free-motion point masses under the influence of  
 106 gravity, the trajectory of a debris-flow nappe can be expressed as follows (Figure 7):

$$107 \quad y = xtg\varphi + \frac{g}{2v_1^2 \cos^2 \varphi} x^2 \quad (2)$$

$$108 \quad x = \frac{v^2}{g} \cos \varphi \left( \sqrt{\sin^2 \varphi + \frac{2gy}{v^2}} - \sin \varphi \right) \varphi \geq 0 \quad (3)$$

108 When  $\varphi = 0$ , equation (2) simplifies to equation (3):

$$x = \sqrt{\frac{2v^2 y}{g}} \quad (4)$$

109 where  $v$  is the initial velocity of the debris flow flowing out of the spillway,  $\varphi$  represents the angle of the  
110 initial velocity in the horizontal direction, and  $y$  is the water elevation difference.

111 Equation (3) indicates that the nappe extension in the horizontal direction 'x' is proportional to the initial  
112 velocity  $v$  and square root of the water elevation difference  $y$ . From Fig. 6 and Table 1, we found that when  
113  $\eta=0.7$ , the nappe extension was longest in the flow direction. From this point of view, a high lateral contraction  
114 ratio increased the distance between the plunge point and the dam toe, which effectively protected the dam  
115 foundation from scouring. The hydraulic characteristics of the nappe away from the spillway at different lateral  
116 contraction ratios were shown in Figure 8 and Figure 9. Figure 8 indicates that increasing the lateral contraction  
117 ratio decreased the width of the debris-flow nappe. Furthermore, the higher lateral contraction of the spillway  
118 strengthened the collision between flows at the spillway outlet. Air bubbles were entrained in the debris flows  
119 when the continuum of the debris flows was broken. Figure 9 shows the extent of the debris-flow nappes. The  
120 distribution of the flow velocity in the vertical direction at the outlet increased with increasing flow depth due to  
121 the effects of boundary friction. Therefore, the longest flow nappes were formed by the debris flows with  
122 relatively large velocities at the flow surface.

#### 123 **4.2 Debris-flow scour features downriver of a check dam**

124 The scour features of debris flows downriver of a check dam represent one of the most important indexes,  
125 which determines the scour depth at the dam foundation. Figure 10 shows the effects of lateral contraction on the  
126 formation of scour holes in an erodible bed. For the same curvature of the spillway surface, decreasing the  
127 contraction ratio decreased the maximum scour depth and caused the location of the maximum scour point to  
128 shift toward the dam toe due to the decreased debris-flow velocity. The maximum scour depth and its location

129 farther from the dam toe for  $\eta=0.7$  were approximately 1.3 and 1.4 times, respectively, larger than for  $\eta=0.4$ .  
 130 Although a high lateral contraction ratio extended the debris-flow nappe, it also increased the scour depth in the  
 131 erodible bed to some extent. In addition, debris-flow density has some effects on the scour depth. Figure 11  
 132 indicates the scour depth caused by debris flow with density of  $1200\text{kg/m}^3$  is a bit larger than that caused by  
 133 debris flow with density of  $1500\text{kg/m}^3$  at a certain lateral contraction ratio (Figure 11). It was explained that the  
 134 debris flow with lower particle concentration (Lower debris-flow density) initialized and carried more bed  
 135 materials than that with higher particle concentration (Higher debris-flow density) when the other factors were  
 136 fixed (Such as longitudinal slope of gully, debris-flow scale, lateral contraction ratio of the spillway).

### 137 4.3 Energy dissipation at different contraction ratios

138 Generally, different energy dissipaters such as the plunge pool (Pagliara et al., 2010; Duarte et al., 2015) or  
 139 step-pool systems (Yu, 2007; Wang et al., 2009; Wang et al., 2012) are required to dissipate the kinetic energy of  
 140 the surplus flow and prevent the dam foundation and riverbed from scouring when sudden changes to the  
 141 channel slope occur. The energy dissipation process of the check dam was estimated using the Bernoulli equation  
 142 (4). The rationale behind using this equation was previously mentioned.

143 The Bernoulli equation between two reference cross-sections is written as follows:

$$Z_1 + h_1 + \alpha_1 \frac{v_1^2}{2g} = Z_2 + h_2 + \alpha_2 \frac{v_2^2}{2g} + h_w \quad (5)$$

144 If  $\Delta Z = Z_1 - Z_2$ , then equation (4) can be transformed into equation (5):

$$\Delta Z + h_1 + \alpha_1 \frac{v_1^2}{2g} = h_2 + \alpha_2 \frac{v_2^2}{2g} + h_w \quad (6)$$

145 The energy dissipation coefficient  $\zeta$  can be expressed as follows:



$$\zeta = 1 - \frac{h_2 + \frac{v_2^2}{2g}}{\Delta z + h_1 + \frac{v_1^2}{2g}} \quad (7)$$

146 where  $Z_1$  and  $Z_2$  are the elevations of reference cross-sections #1 and #2 (Figure. 2b), respectively;  $h_1$  and  $h_2$   
 147 are the depths of debris flows at reference cross-sections #1 and #2, respectively;  $v_1$  and  $v_2$  are the velocities of  
 148 the debris flows at references cross-sections #1 and #2, respectively;  $\alpha_1$  and  $\alpha_2$  are the kinetic energy correction  
 149 coefficients ( $\alpha_1=\alpha_2=1$ ) (Adamkowski et al., 2006);  $\Delta Z$  is the elevation difference between the two reference  
 150 cross-sections; and  $h_w$  is the water head loss.

151 Table 2 indicates that the collision and friction forces between the debris-flow nappes and debris flows in the  
 152 plunge pool dissipated the kinetic energy of the flows, ranging from 42.03% to 78.08% at different contraction  
 153 ratios. In the case of  $V=0.16 \text{ m}^3$ , the energy dissipation rate decreased gradually when the contraction ratio  
 154 changed from 0.7 to 0.4 because the high contraction ratio increased the number of debris-flow collisions when  
 155 it passed through the spillway. In the cases of  $V=0.10 \text{ m}^3$  and  $V=0.06 \text{ m}^3$ , the energy dissipation rate also  
 156 decreased with decreasing the contraction ratios except at  $\eta=0.4$ . The mean value of the energy dissipation rate  
 157 demonstrated a good positive correlation between the energy dissipation rate and the lateral contraction ratio. In  
 158 addition, for the same contraction ratio, the energy dissipation rate increased gradually with decreasing  
 159 debris-flow scale.

#### 160 **4.4 The empirical equation for estimating the maximum scour depth**

161 Many empirical equations have been proposed to predict the maximum scour depth over the last several  
 162 decades (Bormann and Julien, 1991; Zhou, 1991; Adduce et al., 2005; Pan et al., 2013). The main parameters  
 163 include the unit discharge, characteristic particle size of the erodible bed, water elevation difference and clear  
 164 water and debris-flow densities. However, most of the empirical equations (Li and Liu, 2010) neglect  
 165 dimensional homogeneity (the empirical equations should be dimensionally homogeneous). For new type of

166 spillway, the lateral contraction ratio is an important parameter for predicting the maximum scour depth. For a  
 167 debris flow, the maximum scour depth is mainly determined by the following parameters:

$$h_d = f(q, g, \rho_d, \rho_w, d_{90}, \eta, \dots) \quad (8)$$

168 where  $h_d$  is the maximum scour depth,  $q$  is the unit discharge of the debris flow,  $g$  is the acceleration due to  
 169 gravity,  $\rho_d$  and  $\rho_w$  are the debris-flow density and clear water density, respectively (two debris-flow densities  
 170 were considered, including,  $\rho_d=1200\text{kg/m}^3$  and  $\rho_d=1500\text{kg/m}^3$ ),  $d_{90}$  is the characteristic particle size for erodible  
 171 bed materials, and  $\eta$  is the lateral contraction ratio.

172 Based on a dimensional analysis, the dimensionless parameters with clear physical meanings are developed as  
 173 follows:

$$\frac{h_s}{d_{90}} = k \left( \frac{q}{d_{90} \sqrt{g d_{90}}} \right)^{a_1} \left( \frac{\rho_d}{\rho_w} \right)^{a_2} (1-\eta)^{a_3} \quad (9)$$

174 where  $h_s/d_{90}$  is dimensionless scour depth,  $k$  is a coefficient,  $a_i$  is an index ( $i=1, 2, 3$ ),  $\frac{q}{d_{90} \sqrt{g d_{90}}}$  is the  
 175 dimensionless discharge, and  $\rho_d/\rho_w$  is the dimensionless density.

176 According to the experimental data, the regression equation can be expressed as follows:

$$\frac{h_s}{d_{90}} = 3.15 \left( \frac{q}{d_{90} \sqrt{g d_{90}}} \right)^{0.51} \left( \frac{\rho_d}{\rho_w} \right)^{-0.1363} (1-\eta)^{0.7583} \quad (10)$$

177 The regression equation suggests that the flow density had relatively small effects on the depth of the scour  
 178 hole. However, the debris-flow discharge and the lateral contraction had strong effects on the maximum depth of  
 179 the scour hole, which directly determined the kinetic energy of the flow in the downstream erodible bed. The  
 180 validation tests were also performed using the physical experimental model shown in Figure 2, but under  
 181 different conditions. Additional experimental data provided in the literature (Ben and Mossa, 2006) were used to  
 182 verify the reliability of the regression equation. The predicted results exhibited good agreement with the  
 183 experimental results. The absolute error was smaller than 15.0% in most cases, as shown in Figure 12.

184 **4 Conclusions and Discussions**

185 **4.1 Conclusions**

186 The characteristics of debris flows overflowing the new type of spillway were analyzed at different lateral  
187 contraction ratios. The energy dissipation rate and an empirical model for predicting the maximum scour depth  
188 were also studied in this paper. The following conclusions were drawn from this analysis:

- 189 1) Flow patterns were mainly determined by the lateral contraction ratio. At a high lateral contraction ratio, the  
190 spillway effectively extended the debris-flow nappe and increased the distance between the plunge point  
191 and the dam toe. The drop length of the nappe at  $\eta=0.7$  was approximately 1.4 times higher than that at  
192  $\eta=0.4$ .
- 193 2) The plunge pool downriver of a check dam inevitably dissipated the kinetic energy of the debris flow after  
194 overflowing the check dam. The collision and friction between the debris-flow nappe and the debris flow in  
195 the plunge pool dissipated the kinetic energy of the flow, ranging from 42.03% to 78.08% at different  
196 contraction ratios. Generally, increasing the contraction ratio increased the energy dissipation rate at the  
197 same debris-flow scale.
- 198 3) An empirical model was proposed to predict the maximum scour depth downriver of a check dam. The  
199 results indicated that the predicted results exhibited good agreement with the experimental results. The  
200 absolute error was smaller than 15.0% in most cases.

201 **4.2 Discussions**

202 The characteristics of debris flow nape and scour downriver of a check dam with different spillway were  
203 experimentally investigated in this article. When the experimental data are used to predict debris-flow motion  
204 and scour feature downriver of a check dam in prototype, the effects of physical model scale should be  
205 considered. Scaling effect is mainly induced by dissatisfaction of mobility similitude of model sediment in

206 physical model experiments and it leads to discrepancies between the estimated and actual scour results. Just like  
207 the experimental investigation on the scale effect in pier-scour experiments, the bed-particle mobility similitude  
208 (Ettema et al ,1998; Ettema and Melville,1999) or the flow-strength similitude (Lee and Sturm,2009) should be  
209 satisfied to weaken or eliminate the scaling effect for debris-flow scour when the experimental results are  
210 extrapolated to predict prototype performance in the future.

211 When debris flows occur in the mountainous areas with forest the driftwood carried by debris flows is a  
212 common phenomenon. The debris flows combined with driftwood will speed up blockage and jamming of a  
213 check dam. Once the spillway is blocked by the driftwood the subsequent debris flows will overflow from the  
214 crest of a check dam, which will cause extensive scour downriver of a check dam. Therefore, it is also necessary  
215 to investigate the behavior of debris flows with driftwood and propose some reasonable structural or non-  
216 structural countermeasures to mitigate the effects of debris flows with driftwood on the operation of a check dam  
217 in the future.

## 218 **Acknowledgments**

219 The study results presented in this paper were supported by the Key Research Program of the Chinese  
220 Academy of Sciences (Grant No. KZZD-EW-05-01), the National Natural Science Foundation of China (Grant  
221 No.51209195), the Science Technology Service Network Initiative, Chinese Academy of Sciences (Grant No.  
222 KFJ-EW-ST5-094), and the Key Laboratory of Mountain Hazards and Earth Surface Process, Chinese Academy  
223 of Sciences.

## 224 **List of symbols**

- $a_i$  = The index for the dimensionless parameter (-)
- $b$  = The width of the spillway outlet(m)
- $B$  = The width of the spillway inlet (m)
- $d_{90}$  = The characteristic particle size for erodible bed materials (m)
- $k$  = The coefficient for the dimensionless equation (-)
- $h_1$  = The depth of debris flows at reference cross-sections #1 (m)
- $h_2$  = The depth of debris flows at reference cross-sections #2 (m)
- $h_d$  = The maximum scour depth (m)

$h_w$  = The water head loss (m)  
 $g$  = The acceleration of gravity ( $m/s^2$ )  
 $q$  = The unit discharge of the debris flow ( $m^3/s$ )  
 $v$  = The initial velocity of the debris flow flowing out of the spillway( $m/s$ )  
 $v_1$  = The velocity of debris flows at reference cross-sections #1 ( $m/s$ )  
 $v_2$  = The velocity of debris flows at reference cross-sections #2 ( $m/s$ )  
 $V$  = The scale of debris flow in the experiments ( $m^3$ )  
 $x$  = Trajectory in the horizontal direction (m)  
 $y$  = The water elevation difference (m)  
 $Z_1$  = The elevation of reference cross-sections at #1 (m)  
 $Z_2$  = The elevation of reference cross-sections at #2 (m)  
 $\Delta z$  = The elevation difference between the two reference cross-sections (m)

Greek letters

$\alpha_1$  = The kinetic energy correction coefficient for  $v_1$  (-)  
 $\alpha_2$  = The kinetic energy correction coefficient for  $v_2$  (-)  
 $\rho_d$  = The density of debris flows ( $kg/m^3$ )  
 $\rho_w$  = The density of clear water ( $kg/m^3$ )  
 $\zeta$  = The energy dissipation coefficient(-)  
 $\eta$  = The lateral contraction ratio(-)  
 $\varphi$  = The angle of the initial velocity in the horizontal direction( $^\circ$ )

225

226

227       **References**

- 228       Abedini, M., Said, M. A. M., and Ahmad, F.. Effectiveness of check dam to control soil erosion in a tropical  
229           catchment (The Ulu Kinta Basin), *Catena*, 97, 63-70, 2012.
- 230       Adamkowski, A., Janicki, W., Kubiak, J. et al.: Water turbine efficiency measurements using the gibson method  
231           based on special instrumentation installed inside pipelines//Proceedings of the 6th International Conference  
232           on Innovation in Hydraulic Efficiency Measurements, 2006.
- 233       Adduce, C., La Rocca, M., and Sciortino, G.: Local Scour Downstream of Grade Control Structures in Urban  
234           Stream Restoration, Enhancing Urban Environment by Environmental Upgrading and Restoration Nato  
235           Science Series IV: Earth and Environmental Sciences, 43, 307-317, 2005.
- 236       Ben Meftah, M., and Mossa, M.: Scour holes downstream of bed sills in low-gradient channels, *J. Hydraul. Res.*,  
237           44,497-509, 2006.
- 238       Bormann, E., and Julien, P.Y.: Scour Downstream of Grade-control Structures, *J. Hydraul. Eng.*, 117(5), 579-594,  
239           1991.
- 240       Chu, K.J., Hua, Z.L., and Ji, L.J.: Aeration at overflow dams with curved surfaces by different flashboard  
241           spillways, *J. Environ. Eng. Landsc.*, 22(3), 226-236, 2014.
- 242       Cui, P., Zhou, Gordon G.D., Zhu, X.H., and Zhang, J.Q.: Scale amplification of natural debris flows caused by  
243           cascading landslide dam failures, *Geomorphology*, 182,173-189, 2013.
- 244       Duarte, R., Schleiss, A. J., and Pinheiro, A.: Influence of jet aeration on pressures around a block embedded in a  
245           plunge pool bottom, *Environ Fluid Mech.*, 15(3), 673-693, 2015.
- 246       Ettema, R., Melville, B. W., Barkdoll, B.: Scale effect in pier-Scour experiments, *J Hydraul Eng-ASCE.*,  
247           124(6):639-642, 1998.
- 248       Heumader, J.: Technical debris-flow countermeasures in Austria—a review, *Proceedings, Second International*

249 Conference on Debris-Flow Hazards Mitigation: Mechanics, Prediction, and Assessment, 553-564, 2000.

250 Iverson, R. M.: The physics of debris flows, *Rev. Geophys.*, 35(3), 245-296, 1997.

251 Laursen, E. M.: Scale effect in pier-scour experiments, *J Hydraul Eng-ASCE.*, 125(8):894-895, 1999.

252 Lee, S. O., Sturm, T. W.: Effect of Sediment Size Scaling on Physical Modeling of Bridge Pier Scour, *J Hydraul*  
253 *Eng-ASCE.*, 135(10):793-802,2009.

254 Lenzi, M. A.: Stream bed stabilization using boulder check dams that mimic step-pool morphology features in  
255 Northern Italy, *Geomorphology*, 45(3), 243-260, 2002.

256 Lien, H.P.: Design of Slit Dams for Controlling Stony Debris Flows. *Int J Sediment Res.* ,18(1),74-87, 2003.

257 Mizuyama, T.: Structural countermeasures for debris flow disasters, *International Journal of Erosion Control*  
258 *Engineering*, 1(2), 38-43, 2008.

259 Ni, H. Y., Zheng, W. M., and Tie, Y. B.: Formation and characteristics of post-earthquake debris flow: a case  
260 study from Wenjia gully in Mianzhu, Sichuan, SW China, *Nat. hazards*, 61(2),317-335, 2012.

261 Pagliara, S., Roy, D., and Palermo, M.: 3D plunge pool scour with protection measures, *J. Hydro-environ Res.*, 4,  
262 225-233, 2010.

263 Pan, H.L., Wang, R., Huang, J.C., and Ou, G.Q.: Study on the ultimate depth of scour pit downstream of debris  
264 flow check dam based on the energy method, *Eng. Geol.*, 160,103-109, 2013.

265 Remaître, A., Van Asch, T. W. J., and Malet J. P.: Influence of check dams on debris-flow run-out intensity, *Nat.*  
266 *Hazard Earth Sys.*, 8(6), 1403-1416, 2008.

267 Remaitre, A., and Malet, J. P.: The effectiveness of torrent check dams to control channel instability: example of  
268 debris-flow events in clay shales. Check dams, morphological adjustments and erosion control in torrential  
269 streams, Nova Science Publishers Inc., New York, 211-237, 2010.

270 Tang, C., Jiang, Z., and Li, W.: Seismic Landslide Evolution and Debris Flow Development: A Case Study in the

271 Hongchun Catchment, Wenchuan Area of China, *Engineering Geology for Society and Territory*, 2, 445-449,  
272 2015.

273 Toombes, L., Wagner, C., and Chanson, H.: Flow patterns in nappe flow regime down low gradient stepped  
274 chutes, *J. Hydraul Res.*, 46(1), 4-14, 2008.

275 Wang, G. L.: Lessons learned from protective measures associated with the 2010 Zhouqu debris flow disaster in  
276 China, *Nat. Hazards*, 3(69), 1835-1847, 2013.

277 Wang, Z. Y., Melching, C.S., Duan, X.H., and Yu, G.A.: Ecological and hydraulic studies of step-pool systems, *J.*  
278 *Hydraul. Eng.*, 9,705-717, 2009.

279 Wang, Z.Y., Qi, L.J., and Wang, X. Z.: A prototype experiment of debris flow control with energy dissipation  
280 structures, *Nat. Hazards*, 60, 971-989, 2012.

281 Yu, B., Ma, Y., and Wu, Y.: Case study of a giant debris flow in the Wenjia Gully, Sichuan Province, China, *Nat.*  
282 *hazards*, 65, 835-849, 2013.

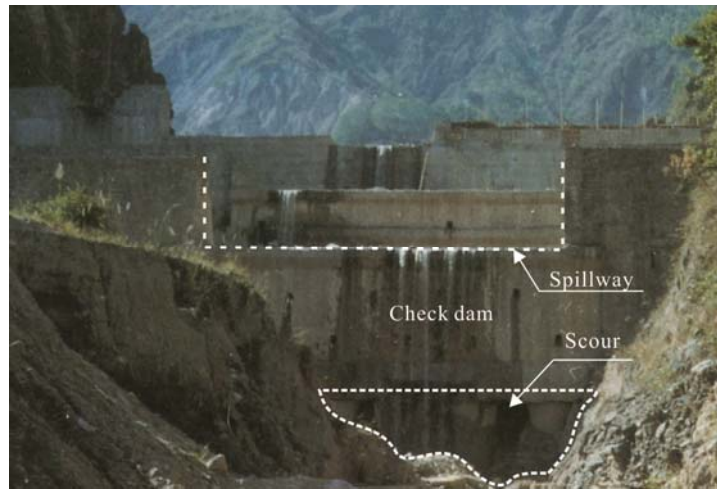
283 Yu, G.A., Wang, Z.Y., and Duan, X.H.: Artificial step-pool system for ecological restoration of a debris-flow  
284 ravine, In: *Proceedings of 32nd IAHR congress, Venice, Italy*, 1-10, July 2007.

285

286



287  
288

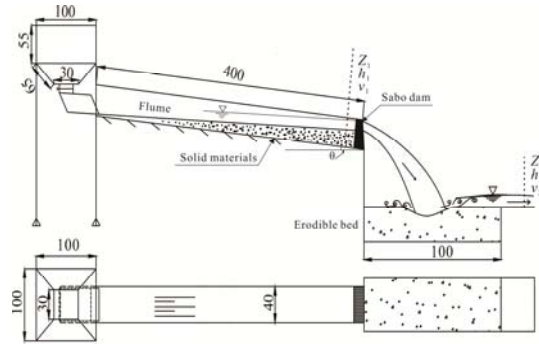


289  
290  
291

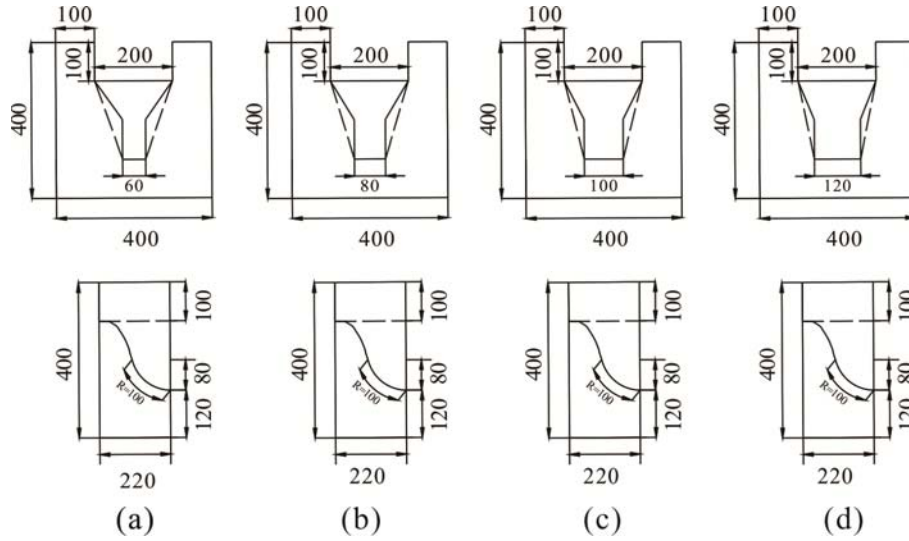
**Fig. 1.** An example of foundation scour downriver of a check dam



(a) Photograph of the experimental setup



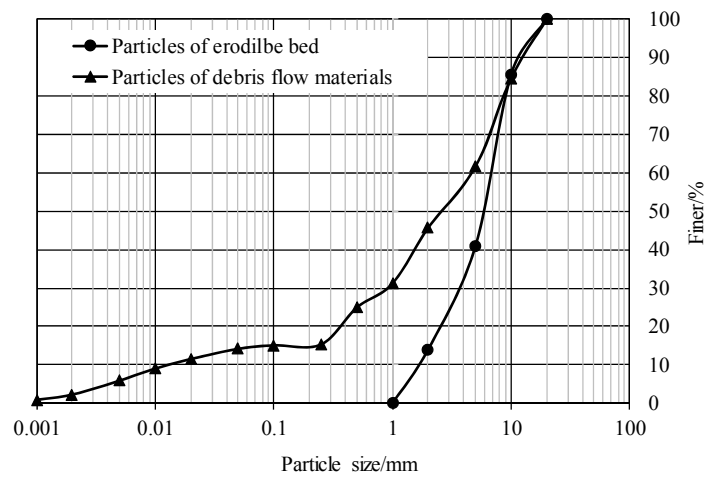
(b) Schematic diagram of the experimental setup (unit: cm)



(c) The structure and dimensions of the spillway (unit: mm). Four different lateral contraction ratios were considered in the experiments: (a)  $B=200.0$  mm,  $b=60.0$  mm,  $\eta=0.7$ ; (b)  $B=200.0$  mm,  $b=80.0$  mm,  $\eta=0.6$ ; (c)  $B=200.0$  mm,  $b=100.0$  mm,  $\eta=0.5$ ; (d)  $B=200.0$  mm,  $b=120.0$  mm,  $\eta=0.4$ . The bottom of the spillway was formed by a compound curve surface (a simple curved segment and a circular segment: radius  $R=100.0$  mm, radius angle  $\delta=75^\circ$ ).

299 **Fig. 2.** Experimental setup

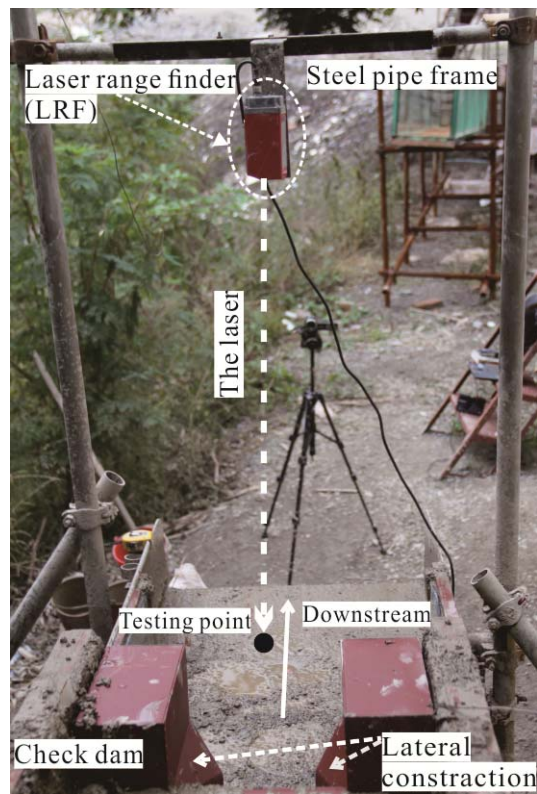
301  
302



303  
304  
305

**Fig. 3.** The particle size distribution of samples for the debris flows and erodible bed

306



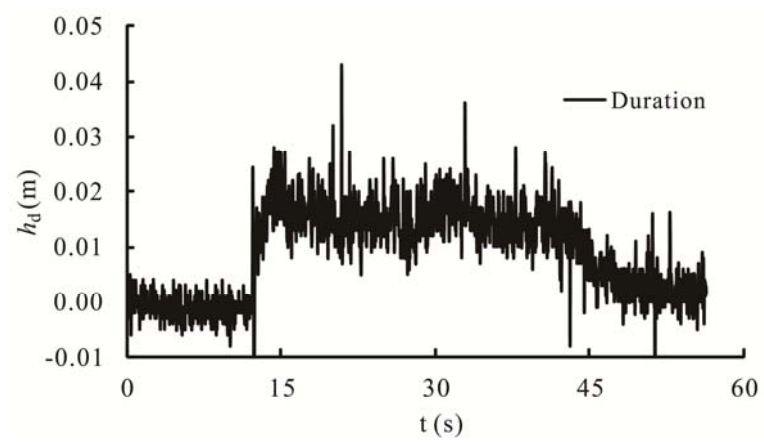
307

308

309

**Fig. 4.** Photograph of the LRF system (the photograph was taken in the downstream direction)

310

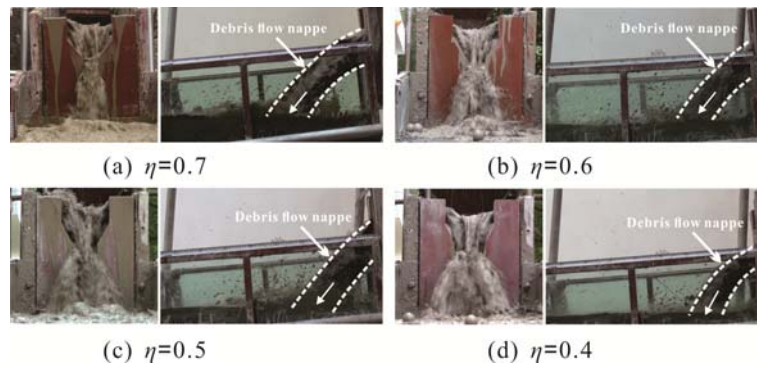


311

312 **Fig. 5.** An example of a debris-flow hydrograph

313

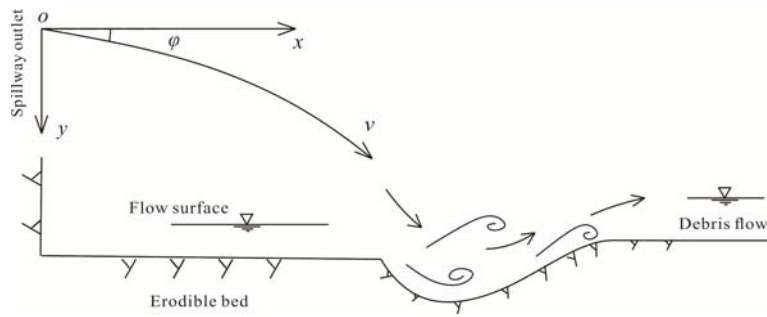
314



315

316 **Fig. 6.** Various debris flow patterns at different lateral contraction ratios (the pictures on the left were taken  
317 from a downstream view)

318



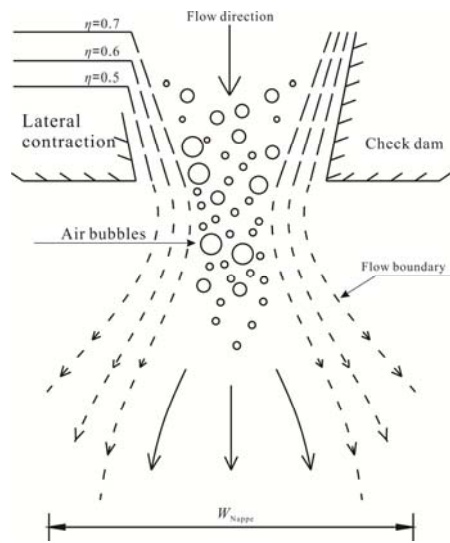
319

320 **Fig. 7.** A diagram of dynamic parameters of debris flows

321

322

323



324

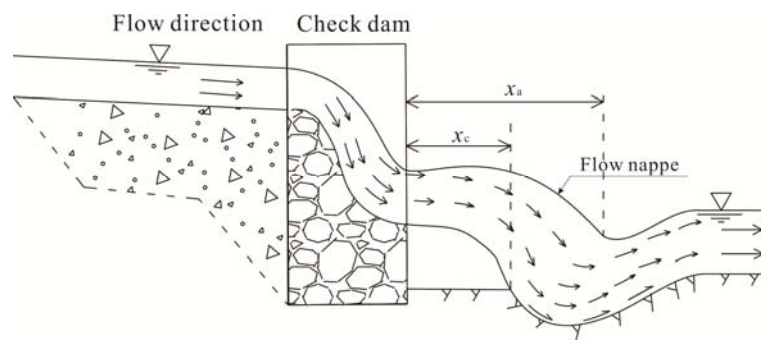
325

**Fig. 8.** The transverse expansion of a debris flow nappe at different lateral contraction ratios

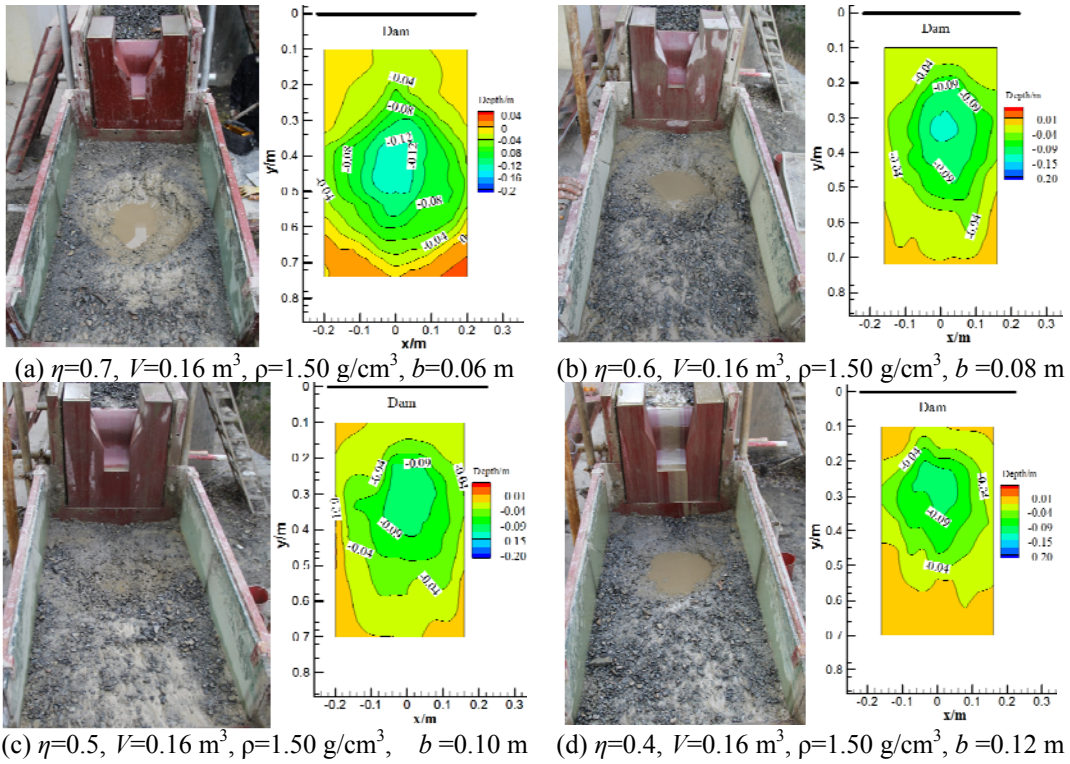
326



327  
328

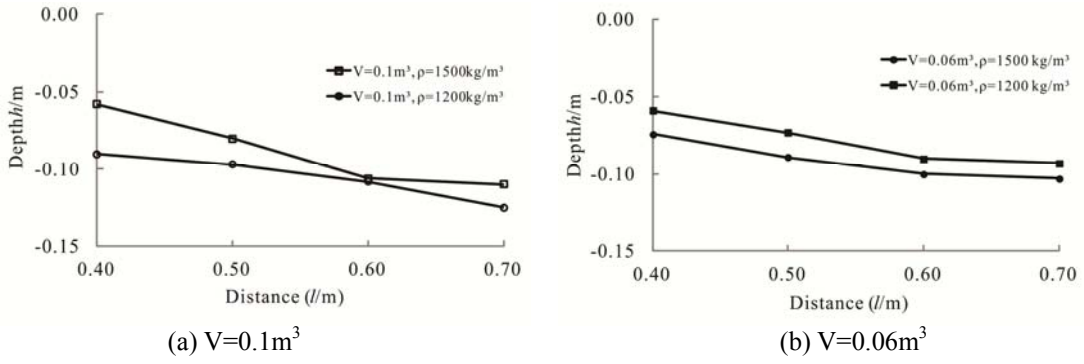


329  
330 **Fig. 9.** The trajectory of a debris flow nappe  
331

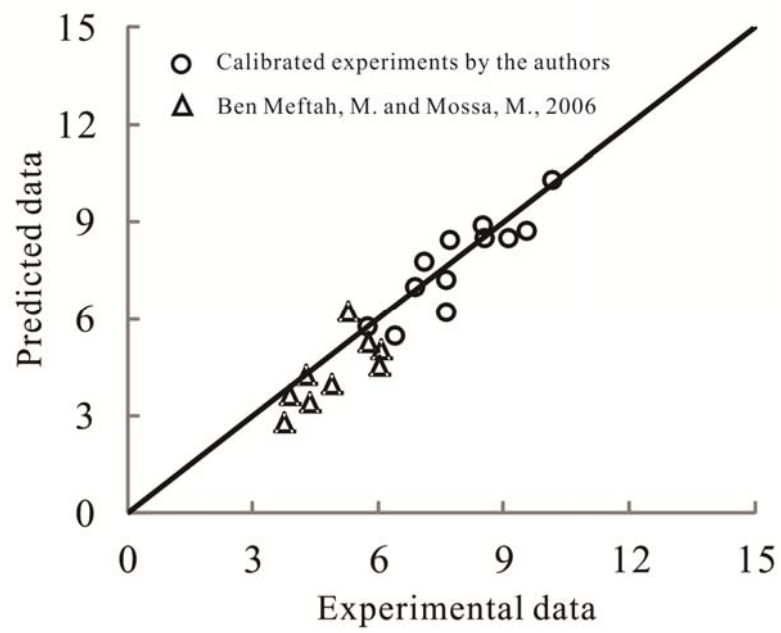


333 **Fig. 10.** The shapes of the scour hole downriver of a check dam ( $V=0.16 \text{ m}^3, \rho=1.50 \text{ g/cm}^3$ )

335  
336



337 **Fig. 11.** Comparison of scour depth at different debris-flow densities  
338



340

341 **Fig. 12.** Comparison between predicted data and experimental ones

342

343 **Table 1.** The main parameters of the debris flow nappe for different contraction ratios

Items	(a)	(b)	(c)	(d)
Width of the outlet $b/\text{mm}$	60.0	80.0	100.0	120.0
Lateral contraction ratio $\eta$	0.7	0.6	0.5	0.4
Width of the nappe $W_{\text{Nappe}}/\text{mm}$	137.2	231.6	292.6	320.6
Broadening ratio $\kappa(\kappa= W_{\text{Nappe}}/b)$	2.29	2.90	2.93	2.67
Length of the nappe away from the outlet $x_a/\text{m}$	0.43	0.34	0.33	0.31
Length of the nappe close to the outlet $x_c/\text{m}$	0.25	0.21	0.21	0.18

344 Notes: B is constant for each spillway type (B =200.0 mm)

345

346 **Table 2.** The energy dissipation rates at different contraction ratios

Scales	Density ( $\rho=1.50 \text{ g/cm}^3$ )			
	$\eta=0.7$	$\eta=0.6$	$\eta=0.5$	$\eta=0.4$
$V=0.16 \text{ m}^3$	66.43%	57.48%	52.34%	42.03%
$V=0.10 \text{ m}^3$	75.37%	72.94%	60.58%	67.97%
$V=0.06 \text{ m}^3$	78.08%	73.70%	63.61%	71.75%
Mean value	73.29%	68.04%	58.84%	60.58%

347

348

349